Free Radical Biology and Medicine 169 (2021) 294–303

Contents lists available at ScienceDirect

Free Radical Biology and Medicine

journal homepage: www.elsevier.com/locate/freeradbiomed

Original article

H-ferritin suppression and pronounced mitochondrial respiration make Hepatocellular Carcinoma cells sensitive to RSL3-induced ferroptosis

Michela Asperti, PhD, Sonia Bellini, Elisabetta Grillo, PhD, Magdalena Gryzik, PhD, Luca Cantamessa, Roberto Ronca, PhD, Federica Maccarinelli, PhD, Alessandro Salvi, PhD, Giuseppina De Petro, PhD, Paolo Arosio, PhD, Stefania Mitola, PhD, Maura Poli, PhD *

Department of Molecular and Translational Medicine, University of Brescia, Brescia, Italy

ARTICLE INFO

Keywords:
Hepatocellular carcinoma
Ferroptosis
Ferritin
RSL3

ABSTRACT

Ferroptosis is a form of regulated cell death dependent on iron, reactive oxygen species and characterized by the accumulation of lipid peroxides. It can be experimentally initiated by chemicals, such as erastin and RSL3, that modulate GPX4 activity, the cellular antioxidant machinery that avert lipid peroxidation. The study aimed to investigate mitochondrial respiration and ferritin function as biomarkers of ferroptosis sensitivity of HepG2 and HA22T/VGH, two Hepatocellular Carcinoma (HCC) cell line models.

Cell viability was determined by 3-(4,5-dimethyl-2-thiazolyl)-2,5-diphenyltetrazolium bromide (MTT) assay, labile iron levels were determined using Calcein-AM fluorescence microscopy, ferritin, glutathione and lipid peroxidation were assayed with commercially available kits. The Seahorse assay was used to investigate mitochondrial function in the cells. The study shows that highly differentiated HepG2 cells were more sensitive to RSL3-induced ferroptosis than the poorly differentiated HA22T/VGH (HCC) cell line (RSL3 IC_{50} 0.07 μM in HepG2 vs 0.3 μM in HA22T/VGH). Interestingly, HepG2 exhibited higher mitochondrial respiration and lower glycolytic activity than HA22T/VGH and were more sensitive to RSL3-induced ferroptosis, indicating a mitochondrial-specific mechanism of action of RSL3. Interestingly, iron metabolism seems to be involved in this different sensitivity, specifically, the downregulation of H-ferritin (but not of L-subunit), makes HA22T/VGH more sensitive toward both RSL3-and iron-induced ferroptosis. Hence only the H-ferritin seems involved in the protection from this cell death process.

1. Introduction

Ferroptosis is characterized by cell membrane damage and integrity loss [1,2] mainly due to the reduction of glutathione peroxidase (GPX4) activity and an accumulation of lipid peroxides [1,3–5]. This occurs in numerous human diseases in which its prevention in neurodegeneration [6,7] or ischemia reperfusion injury [8] or its induction in tumors [9–13], is an interesting therapeutic approach. Since 2012 [1], publications abound on the mechanisms of ferroptosis [14,15], and its induction in tumor cells [16].

Erastin and RSL3 are the most used ferroptosis inducers [1]. Erastin inhibits the cystine-glutamate antiporter (system X_c^-) causing cysteine depletion [1,17] with glutathione (GSH) reduction, necessary for GPX4 activity.

Interestingly, sorafenib, a multikinase inhibitor also inactivates system X_c^- [17,18], and blocks the uptake of cystine, similarly as erastin [12,13]. The effectiveness of sorafenib for the treatment on HCC could be due to its activation of ferroptosis [19–21] in the tumor cells. However, some cells are insensitive to erastin/sorafenib induced ferroptosis because of the capacity to produce cysteine from methionine via transsulfuration pathway [22]. For such cells, RSL3, which directly decreases the enzymatic activity of GPX4 through 14-3-3ε adaptor protein [23–27] can be employed for cancer therapy.

Another target to induce ferroptosis is FSP1 (Ferroptosis Suppressor Protein 1), an oxidoreductase that reduces coenzyme Q10 (CoQ10) [18,19]. Its expression, in combination with GPX4, makes the cells differentially susceptible to ferroptosis. Nevertheless, the role of mitochondria, in cell sensitivity to ferroptosis is still not clearly defined. Mitochondria are morphologically altered during ferroptosis [1] and the ROS scavenger XJB-5-131 targeted to mitochondria was able to block

* Corresponding author.
E-mail addresses: michela.asperti@unibs.it (M. Asperti), maura.poli@unibs.it (M. Poli).

https://doi.org/10.1016/j.freeradbiomed.2021.04.024
Received 20 February 2021; Received in revised form 13 April 2021; Accepted 15 April 2021
Available online 20 April 2021

ferroptosis [20]. RSL3 caused the reduction of mitochondrial membrane potential and mitochondrial respiration, which is prevented by the inhibition of BID or by MitoQ, a mitochondria ROS scavenger [21]. On the other hand, mitochondria-deficient cells are still able to undergo ferroptosis process [22] and it has been reported that mitochondria play a crucial role in cysteine deprivation-induced ferroptosis [23]. Thus, the role of mitochondria in ferroptosis is still controversial and could be different among the cell lines.

Also, the role of iron metabolism in promoting the accumulation of lipid peroxides in ferroptosis, is not yet completely clarified. It is known that iron accumulation in the cells increases ferroptosis occurrence and that it is suppressed by iron chelators [1]. Among iron-related proteins proposed to be connected to ferroptosis [24–32] there is ferritin that, composed by 24 ferritin subunits among H- and L-monomers [33], protects cells from ferroptosis, storing iron in a non-toxic form. Erastin decreased FTH level in mouse fibroblastic cells correlated with the increase of intracellular iron [24]. Moreover the knocking-down FTH in *Drosophila* promoted ferroptosis causing growth defects and adults wings [25] and FTH overexpression in Frataxin knockdown cells rendered cells more resistant to erastin [26]. However, the contribution of the two ferritin subunits, and consequently the role of iron increase in ferroptosis has not been studied yet. The present study aimed to investigate mitochondrial respiration and ferritin function as biomarkers of ferroptosis sensitivity in HepG2 and HA22T/VGH HCC cell lines, both typifying highly- and poorly-differentiated stages of tumor development. The study also investigated the synergy of iron supplementation with ferroptosis inducers to trigger this type of cell death process *in vitro*.

2. Materials and methods

2.1. Antibodies and chemicals

Antibodies: anti-TfR1 (no. 136800, Thermo Scientific, Waltham, MA), anti-Ferroportin (no. NBP1-21502, Novus Biologicals, Littleton, CO), anti-total OXPHOS (no. ab110411, Abcam, Cambridge, UK), anti-cleaved Caspase-3 (no. 9661, Cell Signalling, Denver, MA), anti-FSP1 (no. sc-377120, Santa Cruz Biotechnology, Dallas, TX), anti-β-Actin (no. TA890010, OriGene, Rockville, MD) and anti-GAPDH (no. sc-47724, Santa Cruz Biotechnology). The β-Actin and GAPDH were used for the normalization of the loading. HRP-conjugated secondary antibodies: anti-mouse (no. sc-516102, Santa Cruz Biotechnology) and anti-rabbit (no. A120–101P, Bethyl Laboratories, Montgomery, TX).

Chemicals dissolved in DMSO: RSL3 (1S, 3R-RSL 3, no. S8155) and sorafenib (no. S7397) (Selleck Chemical, Houston, TX); erastin (no. E7781) and Ferrostatin-1 (no. SML0583) (Sigma-Aldrich, Saint Louis, MO); Calcein-AM (no. C-3100), MitoTrackerGreen FM probe (no. M7514), MitoSOX™Red mitochondrial superoxide indicator (no. M36008), JC-1 (5,5′,6,6′-tetrachloro-1,1′,3,3′-tetraethylbenzimidazolcarbocyanine iodide; no. T3168) and C11-BODIPY$^{581/591}$ (no. D3861) (Molecular Probes, Thermo Scientific). Chemicals dissolved in deionised water: ferric ammonium citrate (FAC) (no. F5879), ascorbic acid (no. A4034), Bathophenanthrolinedisulfonic acid disodium salt hydrate (BPS, no. B1375) (Sigma-Aldrich), Desferoxamine (DFO, no. S0080A, Novartis), Deferiprone (DFP, kind gift of Prof. P. Ponka, University of Montreal, Canada). Iron dextran (no. D851, Sigma-Aldrich) was diluted in saline buffer.

2.2. Cell culture

HepG2 (IZSLER, Italy) and HA22T/VGH [34] were cultured in MEM and RPMI-1640 (Gibco, Life Technologies, Carlsbad, CA) respectively and maintained at 37 °C in 5% CO_2. Media are supplemented with 10% FBS, 1 mM sodium pyruvate, 0.04 mg/mL gentamicin, 2 mM L-glutamine and Fungizone (Gibco). The only source of iron is present in FBS.

2.3. MTT assay

Cells seeded in 96-well plate (3×10^3 cells/well) were exposed to chemicals for 24-48-72 h, then incubated with 0.5 mg/mL MTT (3-[4,5-dimethyl-2- thiazolyl]-2,5-diphenyl-2H-tetrazolium bromide, no. M5655, Sigma-Aldrich) for 3.5 h at 37 °C. MTT was substituted with 75 μL DMSO for 15 min at 37 °C under shaking and absorbance measured at 540 nm using Multiskan©EX plate reader (Thermo Scientific).

2.4. ELISA assay

The plates (96-well plates) were coated with 0.1 mL of primary antibody against L-Ferritin (LFO3) or H-ferritin (RH02) (10 μg/mL diluted in 50 mM carbonate buffer pH 9.6) for 18 h at 4 °C. After three washes with PBS-T (phosphate buffer saline with 0.1% Tween20), the wells were over-coated by adding 0.1 mL of 3% BSA diluted in PBS for 1 h at 37 °C. After washing with PBST, 20 μg of protein extract for L-Ferritin analysis (both for HA22T/VGH and HepG2) and 5 or 40 μg of protein extract for H-ferritin analysis (for HA22T/VGH and HepG2, respectively) in duplicate were aliquoted, diluted in 1% BSA-PBST and incubated at 37 °C for 2 h. A standard curve using recombinant human L or H-ferritin was added into the plate, as calibrator. After three washings in PBST, 0.1 mL of anti-L or H-ferritin antibody HRP labelled (diluted 1:500 and 1:200 in 1% BSA-PBST, respectively) were added and plate incubated for 1 h at 37 °C. After three washings in PBST, HRP activity was detected using 1 mg/mL tetramethylbenzene (TMB) dissolved in dimethyl sulfoxide (DMSO) and diluted 1:10 in phosphate-citrate buffer pH 5 with added fresh hydrogen peroxide to final concentration 0.006% and the absorbance read at 620 nm by Multiskan©EX plate reader (Thermo Scientific, Waltham, MA). The reaction was stopped by adding 1 N sulphuric acid and the absorbance was measured at 405 nm. The concentration of ferritins was extrapolated from the calibrator curve and expressed as ng of ferritin/mg of protein extract.

2.5. Labile iron pool assay

The cells ($3 \times 10^{\hat{}4}$) were seeded on 96-well plates and treated with 100 μM FAC or 0.01–0.1–1 μM RSL3 for 16 h. The cells were incubated with 0.25 μM Calcein-AM in MEM with 1 mg/mL BSA for 30 min at 37 °C. After washing, 100 μL of 1X HBSS was added and the fluorescence monitored at an excitation of 488 nm and an emission of 517 nm using EnSight Multimode plate reader (PerkinElmer, Waltham, MA). Cells were then fixed in 4% PFA, stained with Crystal violet solution (0.1% Crystal violet, 20% methanol) and the absorbance at 540 nm used as normalization. The data were expressed as ratio Calcein-AM Fluorescence/Crystal violet absorbance. The Calcein-AM quenching is inversely proportional to the iron concentration.

2.6. Protein extraction and immunoblotting

Proteins obtained using lysis buffer (200 mM Tris-HCl pH 8, 100 mM NaCl, 1 mM EDTA, 0.5% NP-40, 10% glycerol, 1 mM sodium fluoride, 1 mM sodium orthovanadate; Protease Inhibitor Cocktail (Sigma-Aldrich)) were quantified with Micro BCA™ Protein Assay Kit following the manufacturer's instructions (Sigma-Aldrich). Equal protein amounts were separated with SDS–polyacrylamide gel and transferred to a PVDF membrane (Life Technologies). After blocking, the membranes were incubated overnight at 4 °C with primary antibodies and after washes, with secondary antibodies (1 h at RT). The signal was visualized using chemiluminescence PDS kit (GeneSpin, Milan, IT) and CL-XPosure Film (Thermo Scientific). The densitometry was performed using ImageJ software.

2.7. GPX4 activity

The cells from one 75 cm^2 flask or a portion of the tumor xenograft

were lysed on ice in 0.3 mL of lysis buffer (0.1 M KH_2PO_4/K_2HPO_4, 0.15 M KCl, 0.05% (w/v) CHAPS, pH 7.0, containing 1×10^{-3} M 2-mercaptoethanol and a cocktail of protease inhibitors) using a sonicator. Proteins were quantified and 0,2–0,4 mg used for GPX4 activity evaluation. Samples were incubated for 5 min at room temperature in 1 mL of 0,1 M KH_2PO_4/K_2HPO_4, pH 7.8 containing 5×10^{-3} M EDTA, 5×10^{-3} M GSH, 0.1% (v/v) Triton X-100, 0.16×10^{-3} M NADPH and 180 IU/mL Glutathione Reductase (GR). After recording the baseline for 20–30 s, enzymatic activity (expressed as nmoles/min/mg) was triggered by adding 0.025×10^{-3} M phosphatidylcholine hydroperoxide (PCOOH) and quantified as the decrease of absorbance at 340 nm due to NADPH oxidation by GR [35].

2.8. Real Time-PCR

RNA was obtained with TRI Reagent (Sigma-Aldrich) and cDNA generated using ImProm-II™ Reverse-Transcription System kit (Promega, Madison, WI) according to the manufacturer's instructions. Real time-PCR was performed, using iTAq Universal SYBR Green (Promega), according to the manufacturer's instructions, for NCOA4, GPX4, NRF2, NQO1, TxnR1, HO-1 mRNA detection, normalized to HPRT1 and expressed as $2^{-\Delta Ct}$.

2.9. GSH/GSSG ratio

GSH and GSSG were measured using GSH/GSSG-Glo assay detection kit (Promega), following manufacturer's instructions and EnSight Multimode plate reader.

2.10. Lipid peroxidation assay

Cells were treated with 100 μM FAC, 0.05 μM RSL3, 5 μM sorafenib or their combination for 24 h, incubated with 2.5 μM C11-BODIPY$^{581/591}$ for 30 min at 37 °C, fixed with 4% PFA for 15 min at RT and stained with DAPI. The images were acquired using Zeiss Axiovert microscope and SensiCam-PCO Optics (GmbH, Germany).

2.11. Seahorse analyses and mitochondria analysis

Cells seeded in 6-well plates (3×10^5) were treated with 0.1, 1 or 10 μM RSL3. After 16 h, they were collected and incubated in the dark for 20 min at 37 °C with 200 nM MitoTracker Green FM or 10 μg/mL JC-1 or 5 μM MitoSOX™. After washing the cells were suspended in medium and fluorescence detected by MACSQuant Analyzer (MiltenyiBiotec). HA22T/VGH or HepG2 cells ($2 \times 10^{\hat{}4}$ cells/well) were seeded into 24-wells cell culture microplates (Seahorse XFe24 culture plates), Oxygen consumption rate (OCR) and Extracellular acidification rate (ECAR) were measured by Seahorse XFe24 Analyzer (Agilent, Santa Clara, CA). In the experiments with RSL3 after 24 h, HA22T/VGH were treated with 0-0.1–1 μM RSL3 for 16 h (three wells for each condition). The mitochondrial oxidative phosphorylation was analyzed over time before and after sequential injection of 1 μM Oligomycin, 0.5 μM carbonyl cyanide 4-(trifluoromethoxy) phenylhydrazone (FCCP) and 0.5 μM Antimycin A & Rotenone, which inhibit ATPase, the proton gradient, and complex I/III, respectively to enable quantification of basal OCR, ATP-coupled OCR, proton leak, and maximal respiration (Seahorse XF Cell Mito Stress Test, Agilent). At the end of the analysis, cells of each well were trypsinised and counted with Trypan Blue, in a Burker chamber. The data obtained from the measurement of OCR were expressed as pmol/min/1000 cells whereas ECAR was expressed as mpH/min/1000 cells.

2.12. Ferritin KO HA22T/VGH clones

The gRNA for FTH was previously used [28], the gRNA for FTL gene was designed and validated by Feng Zhang's laboratory at the Broad institute. Both gRNAs uniquely target *FTH* or *FTL* genes: *FTH*: GACCATGGACAGGTAAACGT; *FTL*: GGGACTCACCAGAGAGAGGT.

PSpCas9(BB)-2A-Puro (PX459) V2.0 vector (gift from Feng Zhang, Addgene plasmid #62988) [36] was used for both gRNA. HA22T/VGH were transfected using Lipofectamin3000 (Invitrogen), following the manufacturer's instructions. The cells ($2.5 \times 10^{\hat{}5}$) were seeded in 60 mm dish and transfected with 5 μg px459/FTH or px459/FTL using Lipofectamin3000 (Invitrogen), according to the manufacturer's instructions. After 48 h, 1 μg/mL of puromycin (Thermo Scientific) was added and maintained for 72 h. Then the cells were seeded 1 cell per well in a 96-well plate and cultured. Clonal colonies were screened for FTH and FTL expression by ELISA. Genomic alterations were confirmed by Sanger DNA sequencing by BMR Genomics and analyzed in software ChromasLite v2.1. One FTH KO clone was used to generate a double H/L-Ferritin KO clone using px459/FTL.

2.13. Statistical analysis

Statistical significance was assessed by unpaired Student's *t*-test or one/two-way Anova by GraphPad Prism 5 (Inc., La Jolla, CA). p values < 0.05 were considered as significant.

3. Results

3.1. HepG2 are more sensitive than HA22T/VGH to ferroptosis

Cells were treated with RSL3 and erastin (0.1-1-10 μM) for 24-48-72 h (Fig. 1 and Fig. Sup1 A). Erastin 7.5–10 μM caused a viability reduction up to 50% in HepG2 and of 20–40% in HA22T/VGH Fig. Sup1 A-B). The IC_{50} of RSL3 in HepG2 was about 0.5–0.1-0.07 μM (Figs. 1 A) and 0.8–0.5-0.3 μM in HA22T/VGH at 24-48-72 h (Fig. 1 B). The following experiments were focused on RSL3, the inhibitor of GPX4 that resulted reduced by RSL3 0.01–0.1–1 μM in HepG2 and 0.1–1 μM in HA22T/VGH (Fig. 1 E). Notably, Ferrostatin-1 (10 μM) and three different iron chelators BPS, DFP and DFO (100 μM) significantly reduced the effect of 1 μM RSL3 (Fig. 1C and D) confirming that RSL3 induced ferroptosis. Caspase3 cleavage products were absent (Fig. 1 F) indicating the absence of apoptosis.

3.2. RSL3 induced mitochondrial dysfunction

RSL3 increased the mitochondrial ROS, measured with Mitosox probe, (Fig. 2 A), with an anticipated major increase in HepG2. To assess if this ROS production is due to mitochondrial dysfunction, the mitochondrial membrane potential (ΔΨm) was monitored following the JC-1 accumulation. RSL3 caused a significant increase of green JC-1 monomers consistent with reduced mitochondrial ΔΨm (Fig. 2 B), index of depolarized membrane [37], more evident in HA22T/VGH cells (Fig. 2 B). Next, the oxidative phosphorylation complexes were analyzed after 0.1–1 μM RSL3 for 16 h by western blotting (Fig. 2C and E) to understand if the treatments could have an impact also on the mitochondrial subunits that compose the five complexes essential for the normal electron transfer chain. The treatments did not affect HepG2 complexes (Fig. 2C), while in HA22T/VGH they caused a reduction of I-NDUFB8 (Complex I subunit NADH:Ubiquinone Oxidoreductase Subunit B8; 19 kDa), II-SDHB (Complex II subunit succinate dehydrogenase; 30 kDa), III-UQCRC2 (Complex III subunit Ubiquinol-Cytochrome C Reductase Core Protein 2; 48 kDa) and IV-COX-II (Complex IV Cytochrome c oxidase; 22 kDa) (Fig. 2 E), with no significant changes in mitochondrial mass, measured by Mitotracker Green FM probe (Fig. 2 D and F). Since the oxidative phosphorylation complexes were altered after the RSL3 treatment, their mitochondrial function was evaluated using Seahorse Mito-Stress Test to detect basal respiration, ATP-linked respiration and maximal respiration measuring the oxygen consumption rate (OCR) after RSL3 (0.1–1 μM) for 16 h. The extracellular acidification rate (ECAR) was measured as a readout of the glycolytic activity. The spare respiratory capacity, ATP-linked respiration and maximal respiration of

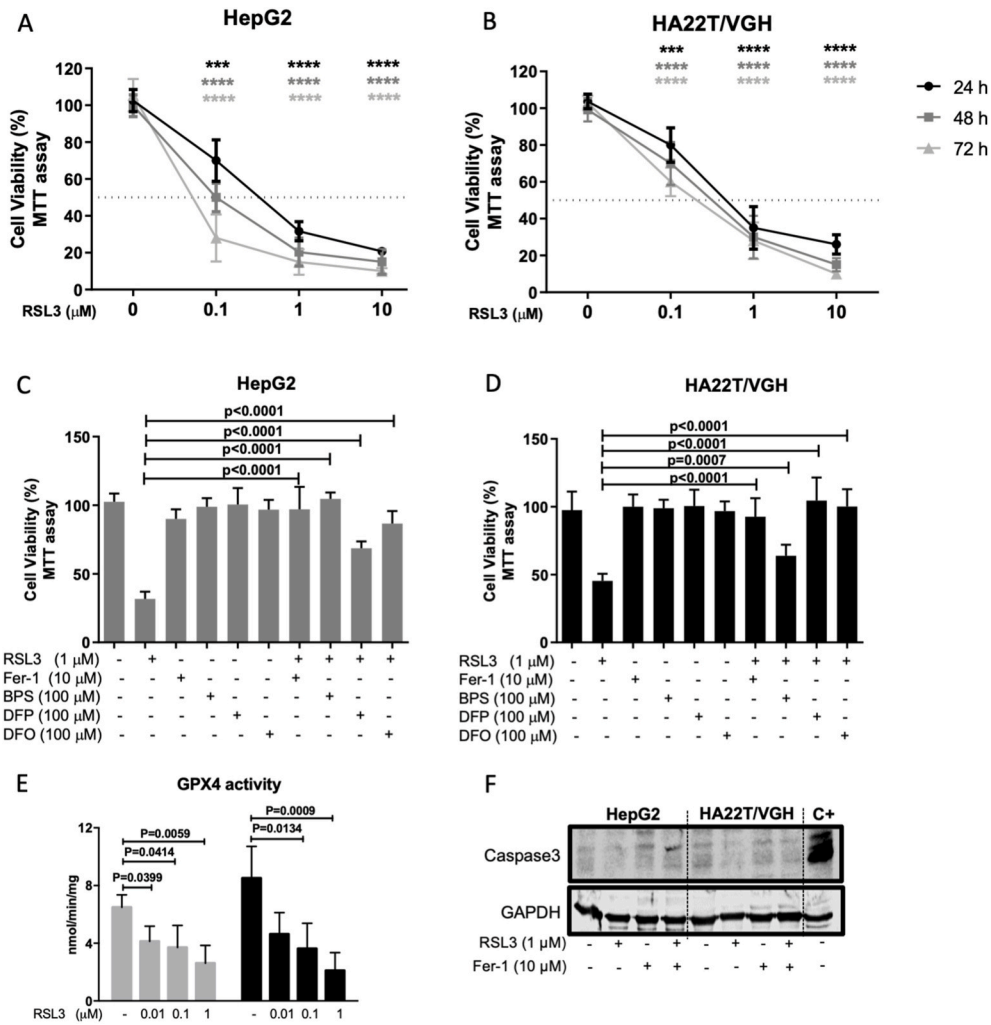

Fig. 1. RSL3 induced ferroptosis with a reduction in cell viability more evident in HepG2 than HA22T/VGH. (A) and **(B)** MTT assay after the treatment with different concentrations (0.1-1-10 μM) of RSL3 in HepG2 **(A)** and HA22T/VGH **(B)** cells (N = 4). **(C)** and **(D)** MTT assay after 24 h treatment with RSL3 1 μM in HepG2 (grey histograms) **(C)** and in HA22T/VGH (black histograms) **(D)** in combination with Ferrostatin-1 (Fer-1, 10 μM) or 100 μM iron chelators BPS, DFP and DFO (N = 3). **(E)** GPX4 activity (expressed as nmol/min/mg) in HepG2 (grey histograms) and HA22T/VGH (black histograms) treated with RSL3 (0.01–0.1–1 μM) (N = 3). *P* values were obtained by one-way ANOVA. **(F)** Western blotting on cleaved-caspase3 (caspase3 in the figure) in HepG2 and HA22T/VGH treated with RSL3 (1 μM) and/or Ferrostatin-1 (10 μM); C+ is a positive control (treated with 2 μM Staurosporine for 4 h). P values were obtained by two-way ANOVA, comparing each dose of RSL3 to the untreated cells (0) for each time point (24 h, black stars; 48 h, dark grey stars; 72 h, light grey stars, for figures A and B) or P values are shown on the graphs. The stars *, **; *** and **** correspond to a P value of ≤0.05; ≤0.01; ≤0.001; ≤0.0001 respectively.

HA22T/VGH were significantly reduced in a dose dependent manner while glycolytic activity was not significantly affected (Fig. 2 G). Altogether the data indicate a specific RSL3 activity on the mitochondria.

3.3. Iron-related proteins are not affected by RSL3

The labile intracellular iron (LIP) in HA22T/VGH was monitored using Calcein-AM assay. The treatment with RSL3 0.1 and 1 μM caused a decrease of Calcein fluorescence indicating an increase of free iron that quenched its fluorescence, as observed after 100 μM FAC treatment (Fig. Sup2 A). However, RSL3 did not affect L- and H- ferritins (Fig. Sup2 B), ferroportin and TfR1 (Fig. Sup2 C) (in contrast with what reported for TfR1 in Huh-7 cells [30]).

3.4. High mitochondrial respiration increases ferroptosis susceptibility

To study the higher sensitivity of HepG2 compared to that of HA22T/VGH, their mitochondrial respiration and glycolytic activity were explored. HepG2 showed a more pronounced oxidative phosphorylation (oxphos) than HA22T/VGH, expressed as an increase of OCR in basal conditions (Fig. 3 A) and ATP-linked respiration, spare respiratory capacity and maximal respiration (Fig. 3 A). Conversely, the glycolytic activity of HepG2 was lower compared to HA22T/VGH cells, as indicated by a lower ECAR (Fig. 3 A). In keeping with their higher oxphos activity, HepG2 cells exhibit higher content of the respiratory chain complexes (Fig. 3 B) to that of HA22T/VGH. However, HepG2 have a lower mitochondrial mass than HA22T/VGH (Fig. 3C). Together, these data suggest that cells with highly efficient mitochondria may be more susceptible to RSL3.

3.5. HA22T/VGH cells express high level of iron related proteins and antioxidant enzymes

Some relevant iron related proteins and the antioxidant machinery were analyzed in order to verify if the differences of iron availability could contribute to ferroptosis susceptibility. HA22T/VGH showed higher levels of TfR1 and FPN (Fig. 4 A) than HepG2 cells. Likewise, L- and H-ferritins were higher in HA22T/VGH compared to HepG2 (L-Ferritin: 140 *vs* 20 ng/mg; H-ferritin: 120 *vs* 2.1 ng/mg) (Fig. 4 B) with a reduced LIP in HA22T/VGH (Fig. 4C). Transcription levels of *NCOA4* were similar in both cell lines, whereas *Hepcidin* was very low in HA22T/VGH (Fig. 4 D). This suggests a more active system to control iron metabolism in HA22T/VGH optimizing the iron intake and protecting from its toxicity (Fig. 4 D) as demonstrated by higher expression of some antioxidant enzymes (HO-1, TxnR1, HSBP1 and NQO1) (Fig. Sup3 A). GPX4 showed a significant tendency to be more active in HA22T/VGH (Fig. Sup3 B) supported by the lower GSH/GSSG ratio compared to that of HepG2 (Fig. Sup3 C), whereas levels of FSP1 were similar (Fig. Sup3 D).

3.6. H-ferritin KO HA22T/VGH are more sensitive to RSL3 than the wild type cells

To verify if the high levels of ferritins in HA22T/VGH (Fig. 4 B) may

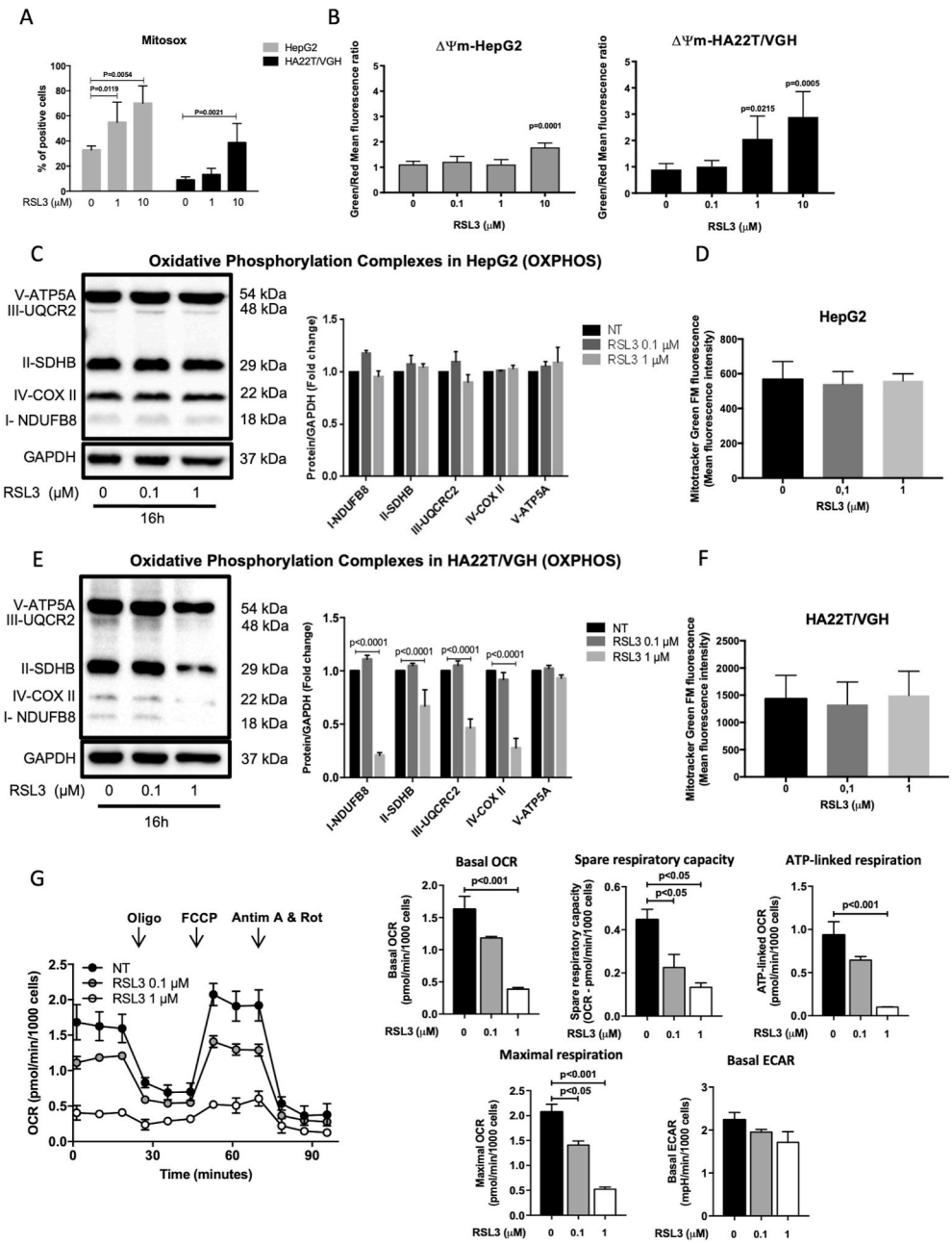

Fig. 2. The treatment with RSL3 induced changes in Oxidative Phosphorylation and mitochondrial respiration. (A) Mitosox assay after the treatment with RSL3 (1 and 10 μM) for 16 h of HepG2 (grey histograms) and HA22T/VGH (black histograms) (N = 3). **(B)** JC-1 probe evaluation by cytofluorimeter after the treatment of HepG2 and HA22T/VGH cells with RSL3 (0.1-1-10 μM) (N = 3). The graphs derived from the ratio between the green and the red fluorescence of the probe. **(C)** and **(E)** WB for the 5 Oxidative Phosphorylation proteins (I-NDUFB8: Complex I subunit NADH:Ubiquinone Oxidoreductase Subunit B8. II-SDHB: Complex II subunit succinate dehydrogenase. III-UQCRC2: Complex III subunit Ubiquinol-Cytochrome C Reductase Core Protein 2. IV-COX-II: Complex IV Cytochrome c oxidase. V-ATP5A: Mitochondrial membrane ATP synthase (F (1)F (0) ATP synthase) in mitochondria and the densitometry normalized for GAPDH in HepG2 **(C)** and HA22T/VGH **(E)** (N = 3). **(D)** and **(F)** Mitochondria in HepG2 **(C)** and HA22T/VGH **(E)** cells analyzed by MitotrackerGreen FM probe with cytofluorimeter after treatment with RSL3 (0.1–1 μM) for 16 h (N = 3). **(G)** Seahorse analysis for the respiration as OCR and ECAR in HA22T/VGH cells after treatment with RSL3 (0.1 and 1 μM) for 16 h (N = 2). *P* values were obtained comparing the not treated cells (NT or 0) with the treated ones, by one-way ANOVA.

protect them from ferroptosis, knockout clones for H-, L- and both H/L-subunit were produced using CRISPR/Cas9 technology, obtaining 2 clones without H-ferritin (KO–H C16 and KO–H C19; Fig. Sup4 A and C), 2 clones without L-Ferritin (KO-L B9 and KO-L C5; Fig. Sup4 B and D) and 2 clones without both H/L-Ferritin (KO–H/L B11 and KO–H/L E9; Fig. Sup3 A-D). ELISA assay confirmed the lack of the specific ferritin in the selected clones (Fig. Sup4 D). Interestingly, the KO–H C16 and C19 clones showed about 3-fold higher level of L-Ferritin than wild type (WT) cells, possibly due to a compensatory mechanism (Fig. Sup4 D). All the clones were treated with RSL3 (0.01–10 μM) for 24 h. The KO–H C16 and KO–H C19 clones showed significantly higher sensitivity to RSL3 than C6 WT clone (Fig. 5 A). In fact, at 0.05 and 0.1 μM both KO–H showed 50–70% reduction of cell viability compared to WT cells. In contrast, the KO-L B9 and KO-L C5 clones were as resistant as WT (Fig. 5 A). The double KO had the same pattern as KO–H cells (Fig. 5 A). The RSL3 IC_{50} at 24 h in H-ferritin-KO clones was about 0.05 μM compared to 0.8 μM of WT and L-Ferritin-KO cells. Interestingly, the co-treatment with Ferrostatin-1 or DFO significantly reduced the effect of RSL3 (Fig. 5 B) indicating that the viability loss of H-ferritin KO clones was due to ferroptosis. These data support that H-ferritin are important in the protection from ferroptosis and that the H-ferritin content may predict their sensitivity to it.

3.7. Iron induces ferroptosis in H-ferritin KO HA22T/VGH cells

HA22T/VGH clones were treated with FAC 0.5-1-5 mM for 72 h. This had a minor effect on the WT and L-ferritin KO clones causing a decrease in cell viability only at 5 mM. In contrast, the KO–H clones showed a high sensitivity to iron overload with a 50–80% reduction of their viability with 1–5 mM FAC, respectively (Fig. 5 C, red and orange histograms). The double KO cells showed a pattern similar to that of H-ferritin KO cells (Fig. 5 C, purple and pink histograms). The combination 5 mM FAC plus 10 μM Ferrostatin-1 (Fig. 5 D) rescued almost completely the cell viability (Fig. 5 D, red and orange histograms) confirming that

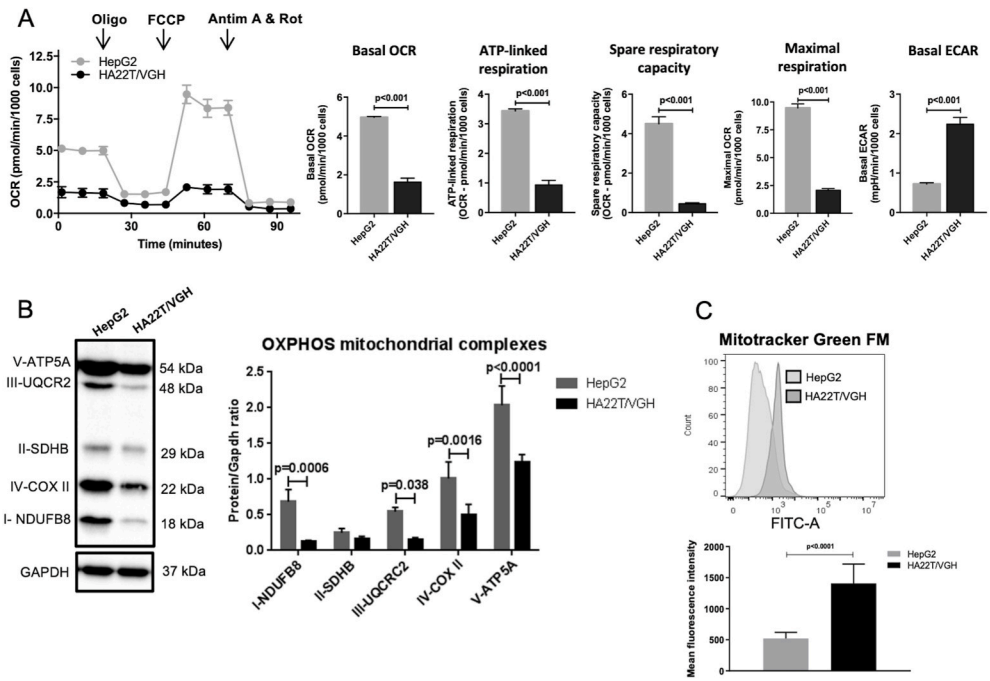

Fig. 3. Respiration capacity of HepG2 and HA22T/VGH cell lines. (A) Seahorse analysis for the respiration as OCR and ECAR in HA22T/VGH and HepG2 cells. **(B)** Western Blotting for mitochondrial complexes and GAPDH in HA22T/VGH and HepG2 cells (I-NDUFB8: Complex I subunit NADH:Ubiquinone Oxidoreductase Subunit B8. II-SDHB: Complex II subunit succinate dehydrogenase. III-UQCRC2: Complex III subunit Ubiquinol-Cytochrome C Reductase Core Protein 2. IV-COX-II: Complex IV Cytochrome c oxidase. V-ATP5A: Mitochondrial membrane ATP synthase (F (1)F (0) ATP synthase). Densitometry was performed using ImageJ and the values (N = 3) were normalized to GAPDH as indicated. **(C)** Mitochondria in HepG2 and HA22T/VGH cells visualized by MitotrackerGreen FM probe with cytofluorimeter (N = 3). In A, B and C, HepG2 are grey histograms and HA22T/VGH black histograms and *P* values were obtained by one-way ANOVA.

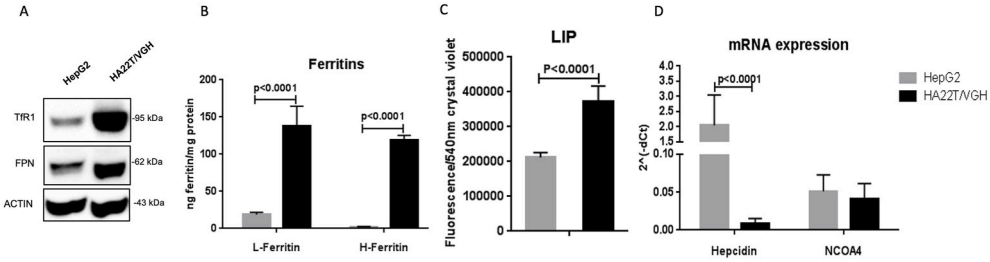

Fig. 4. HA22T/VGH expressed high level of TfR1, FPN and Ferritins compared to HepG2 cells. (A) Western Blotting on TfR1 and FPN; β-Actin is used as a loading control. **(B)** ELISA for L- and H-ferritin in HepG2 (grey histograms) and HA22T/VGH (black histograms) cells (N = 3). **(C)** Labile iron pool detected by Calcein-AM assay in HepG2 (grey histograms) and HA22T/VGH (black histograms) cells (N = 3). The values are expressed as ratio between the fluorescence detected and the absorbance at 540 nm after Crystal violet normalization. **(D)** qPCR for Hepcidin and NCOA4 mRNAs in HepG2 (grey histograms) and in HA22T/VGH (black histograms) cells. The mRNA levels are expressed as 2^(-dCt) related to HPRT1 (N = 3). *P* values were obtained by one-way ANOVA.

iron alone can induce ferroptosis in H-ferritin deficient cells.

3.8. *RSL3, iron and sorafenib co-treatments increase the susceptibility to ferroptosis*

Co-treatment of cells with iron, sorafenib and RSL3 could shed light on the effectiveness of their interactions to enhance the sensitivity of HCC cells to ferroptosis.

The cells were treated with sorafenib (5 μM), RSL3 (0.1 μM), and FAC (100 μM) in different combinations for 24 and 72 h. As shown in Fig. 6, sorafenib alone for 24 h had a little effect, but in co-treatment with RSL3 (Fig. 6 A–B) the cell viability was reduced of 60% in HepG2 (Figs. 6 A), and 20% in HA22T/VGH (Fig. 6 B). Moreover, the triple combination induced an even higher viability loss (70% HepG2 and 60% HA22T/VGH; Fig. 6 A and B). At 72 h the same trend was observed for both cell lines: the co-treatment with sorafenib and RSL3 potentiates the cell death with 80% (HepG2) and 60% (HA22T/VGH) of cell viability reduction, while the triple treatments caused a 90% and 80% cell death, respectively (Fig. 6 C and D). In addition, the combination RSL3 and FAC was also effective in both cell lines with a significant increase of cell death compared to the single treatment (Fig. 6A–D). These results support the efficacy of the co-treatment and that the intracellular iron level could increase the cell sensitivity to ferroptosis. Finally, the increase of C11-BODIPY$^{581/591}$ probe oxidation was evaluated. As shown in Fig. 6 E, all treatments increased the green fluorescence thus meaning an augmented lipid ROS formation and supporting the ferroptotic cell death (Fig. 6 E).

4. Discussion

Ferroptosis is characterized by high levels of intracellular iron, reduction of antioxidant machinery and lipid peroxides production [1]. Tumor cells are sensitive to it, due to their high level of intracellular iron and increased oxidative stress status compared to normal cells. However, it is known that different tumors show different sensitivity towards ferroptosis, depending on their differentiation stage, gene expression and metabolism [38,39]. HCC represents the sixth most common cancer [40] and the fourth cause of cancer-related deaths in the world [41], and new therapeutic strategies are required to overcome the resistance often developed to the present therapy. Recent studies have shown that genetic and mainly metabolism alterations are involved in the progression of HCC and in its differentiation stage [42–45]. Interestingly, it is known that in HCC the glycolysis, pentose phosphate pathway and fatty acid (FA) synthesis are increased while the Tricarboxylic Acid (TCA) cycle as well the beta-oxidation are suppressed [45]. Moreover, the FA synthesis and uptake are more pronounced in highly differentiated HCC compared

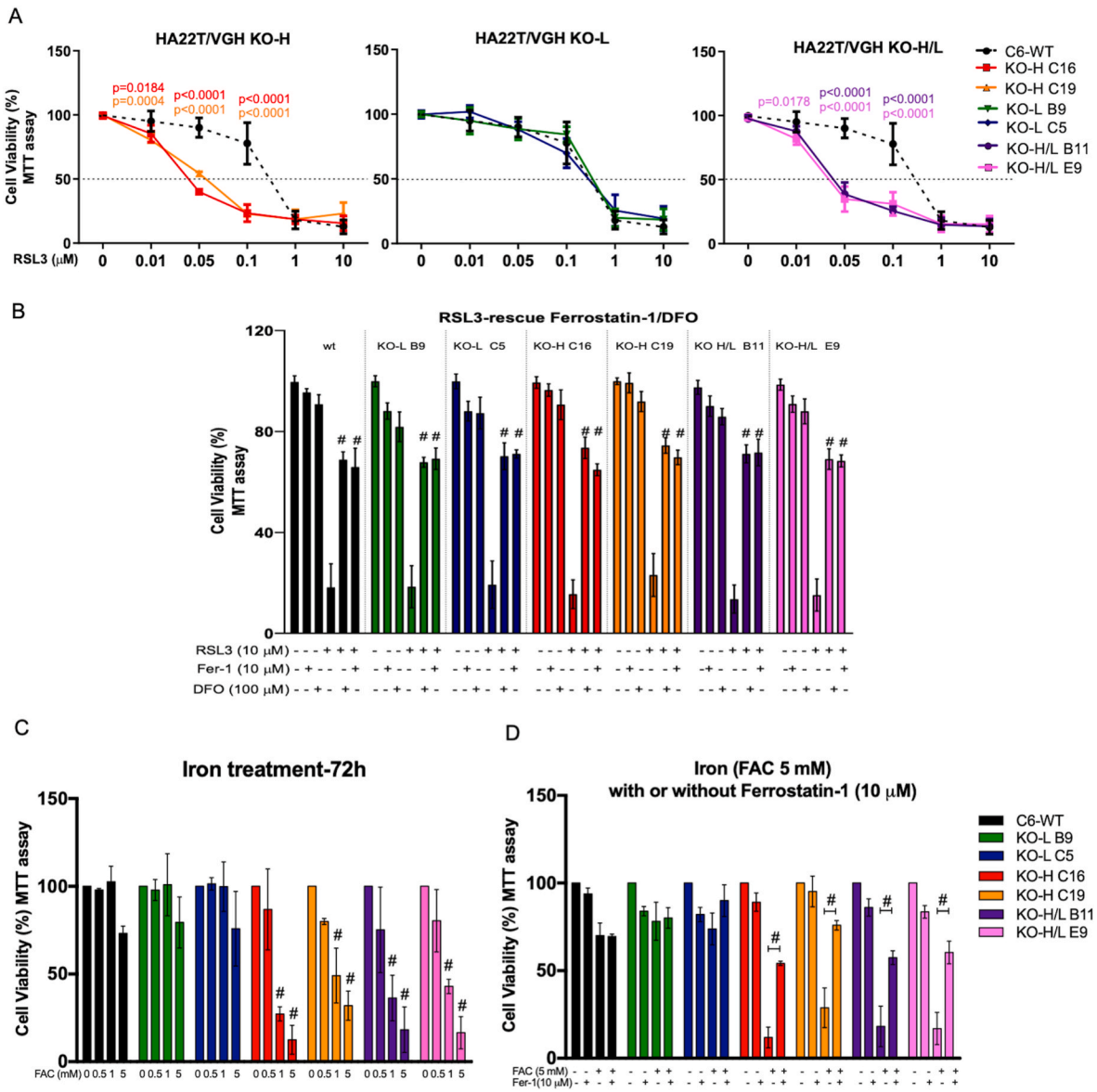

Fig. 5. HA22T/VGH ferritin-H KO cells are more sensitive to RSL3-induced ferroptosis than the WT and ferritin-L KO ones. (A) MTT assay after the treatment with different concentrations of RSL3 (0.01–0.05-1-10 μM) for 24 h of HA22T/VGH WT, KO–H C16 and C19, KO-L B9 and C5, KO–H/L B11 and E9 clones (N = 3). **(B)** MTT assay after 24 h treatment of HA22T/VGH WT, KO–H C16 and C19, KO-L B9 and C5, KO–H/L B11 and E9 clones with RSL3 10 μM in combination with Ferrostatin-1 (10 μM) and 100 μM iron chelator DFO (N = 3). **(C)** MTT assay after 72 h treatment of HA22T/VGH WT, KO–H C16 and C19, KO-L B9 and C5, KO–H/L B11 and E9 clones with FAC (0.5-1-5 mM) (N = 3). **(D)** MTT assay after 72 h treatment of HA22T/VGH WT, KO–H C16 and C19, KO-L B9 and C5, KO–H/L B11 and E9 clones with FAC (5 mM) in combination with Ferrostatin-1 (10 μM) (N = 3). *P* values were obtained by one-way ANOVA and are shown in the graph in A) whereas in B), C) and D) the symbol # corresponds to a *P* value of ≤0.0001.

to the poorly differentiated ones, leading to a modification of the lipid bilayer membrane and possibly to the FA accumulation [45]. Depending on the level of polyunsaturated fatty acids (PUFAs) in this lipid accumulation, these features suggest that: first, HCC could be sensitive to ferroptosis, a lipid peroxidation dependent cell death; second, highly differentiated HCC could show even higher sensitivity to ferroptotic cell death, due to the presence of more lipid substrates which are targets of the peroxidation. Accordingly, the study shows that HepG2 and HA22T/VGH HCC cells that recapitulate the highly- and poorly-differentiated stages of the tumor, respectively [59][60], are sensitive to ferroptosis inducers, erastin and RSL3, with the highly differentiated HepG2 cells the most sensitive ones (RSL3 IC_{50} 0.07 μM in HepG2 vs 0.3 μM in HA22T/VGH). This suggests a correlation with the lipid accumulation in the highlydifferentiated HCC and increased sensitivity to ferroptosis cell death.

Another important aspect to take into account, as recently published [45], is that the glycolytic activity is more pronounced in poorlydifferentiated HCC whereas the TCA cycle was downregulated, suggesting that the Warburg effect become more pronounced with the decreased level of tumor cell differentiation. As shown by Seahorse analysis, the treatment with RSL3 reduced the mitochondrial membrane potential and the respiratory capacity in a dose dependent manner, without interfering with the glycolytic activity. Interestingly, cells with high mitochondrial activity that produce ATP preferably via mitochondrial respiration, like HepG2 cells, are more susceptible to RSL3. Altogether the data indicate a specific RSL3 activity on the mitochondria functionality that could be an important aspect to be considered in the choice of ferroptosis inducers based on the type and the differentiation stage of the tumor.

In addition, the study shows that intracellular iron is involved in the

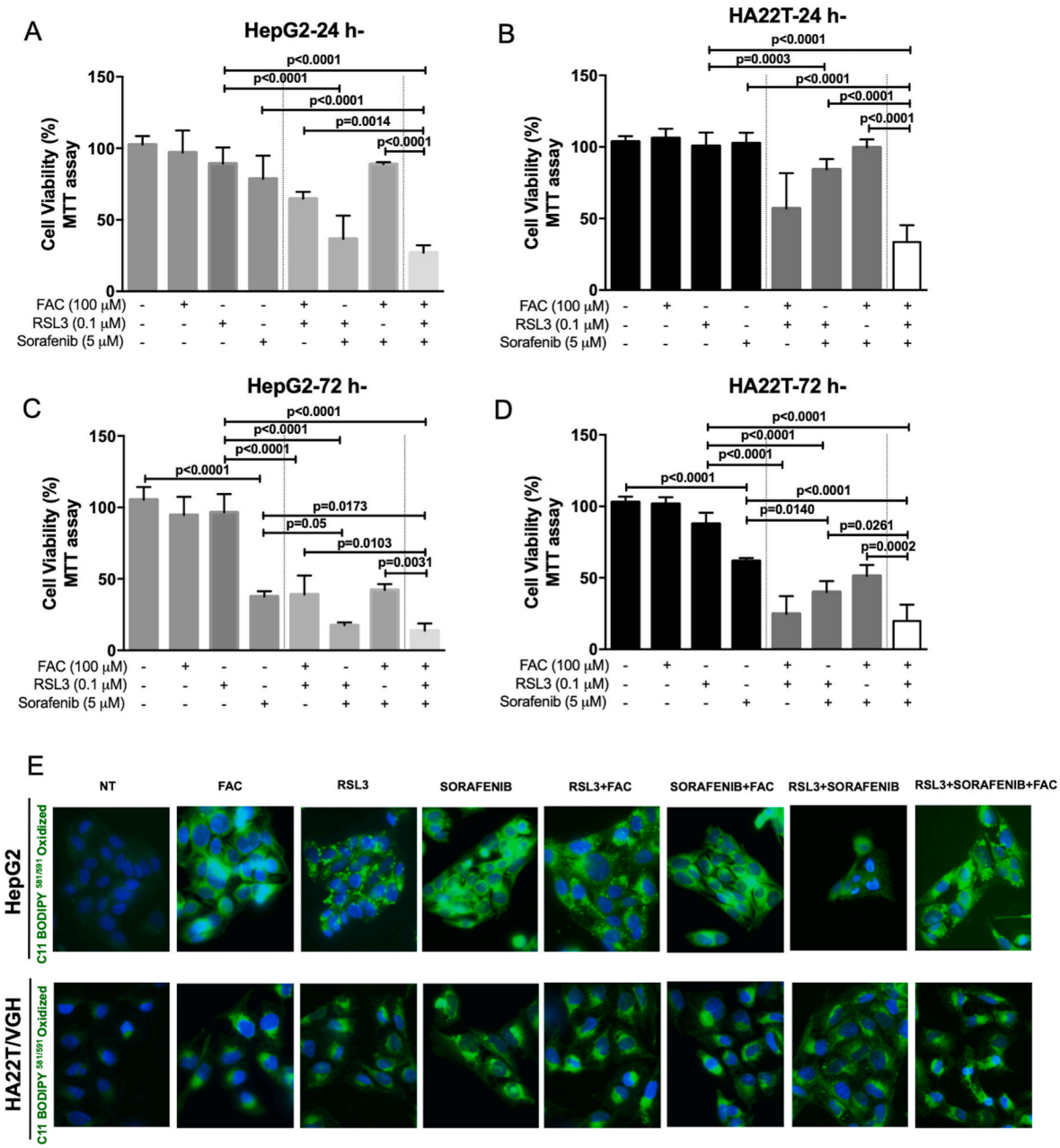

Fig. 6. The combination of treatments with sorafenib, RSL3 and FAC is more effective in reducing cell viability than single treatments in HepG2 and HA22T/VGH cells. (A) and **(B)** MTT assay after 24 h, **(C)** and **(D)** after 72 h of RSL3 (0.1 μM), sorafenib (5 μM) and FAC (100 μM) in single treatment or in combination in HepG2 **(A–C)** and HA22T/VGH **(B–D)** cells (N = 3). *P* values were obtained by one-way ANOVA. **(E)** Cells were treated with 100 μM FAC, 0.05 μM RSL3 or 5 μM sorafenib alone or in combination for 24 h and the lipid ROS formation was monitored using C11-BODIPY$^{581/591}$ probe in fluorescent microscope. DAPI dye was used to stain nuclei. Images were taken with 63× magnification (with immersion) using FITC and DAPI filters to visualize the oxidized probe (in green) and the nuclei (in blue) respectively. (For interpretation of the references to colour in this figure legend, the reader is referred to the Web version of this article.)

execution of ferroptosis and the highlydifferentiated HepG2 cells showed a lower level of all the proteins involved in the control of iron metabolism (TfR1, FPN and ferritin) and a higher level of intracellular labile iron pool (LIP), compared to the poorly differentiated HA22T/VGH cells. These characteristics exposed HepG2 cells to a toxic effect of iron when the antioxidant machinery is compromised, due to RSL3 or erastin treatment. This is evaluated also *in vivo* in a preliminary experiment (Fig. Sup5) and the preliminary findings showed that the growth of xenograft HCC tumors (using HepG2 cells), treated with RSL3 *plus* iron dextran was significantly reduced compared to untreated group or treated with RSL3 or iron dextran alone, suggesting that the combination of ferroptosis inducers and iron could be a promising strategy to treat HCC. Of course, this *in vivo* experiment needs to be optimized and the results confirmed, increasing the number of mice and introducing sorafenib treatment, in order to mimic the promising results obtained *in vitro* where the triple treatment (RSL3-iron-sorafenib) significantly reduced the cell viability, in both highly and poorly differentiated cell lines.

Among the proteins involved in iron metabolism, ferritin, is strictly related to the intracellular iron content, even if a clear correlation of its subunits (H- and L-chain) and ferroptosis sensitivity is not yet fully demonstrated [24,25,27,31,32]. H-ferritin, with its ferroxidase activity, is able to convert Fe^{2+} to Fe^{3+} whereas L-ferritin is dedicated to the iron nucleation inside the ferritin shell [33,46]. The study showed that only

H-ferritin is important for ferroptosis process in HCC. In fact, HA22T/VGH cells, with higher levels of both L- and H-ferritin subunits compared to HepG2 cells, could be more protected from ferroptosis. This was proved by the fact that only the downregulation of H-ferritin in HA22T/VGH was able to sensitize the cells to ferroptosis and the consequent increase of L (as a compensatory mechanism) cannot protect them. Interestingly, in H-ferritin KO cells, iron alone was able to trigger ferroptosis, making ferritin and iron content, two important parameters to take into account in the execution of ferroptosis. Altogether these results suggest that the down regulation of H-ferritin, with the direct increase of LIP, supports the lipid peroxidation in ferroptosis independently to the inducer used. On the other hand, our previous results, showed that in Hela cells the down regulation of NCOA4 (meaning less ferritinophagy and thus less ferritin degradation) increased the cell resistance to erastin but reduced that one to RSL3 [29], suggesting a more complex role of NCOA4 in ferroptosis. Interestingly, it was published that the NCOA4 downregulation induces mitochondrial disfunctions in Hela cells [47] opening new hypothesis to understand the increased sensitivity of NCOA4 KO cells toward RSL3 but more studies are required to clarify this aspect.

Finally, ferroptosis is a very complex type of cell death regulated by cellular metabolism that at least in HCC cells seems to involve mitochondrial respiration, H-ferritin content and lipid accumulation. These features make the highly differentiated HCC cells (with high mitochondrial respiration, low H-ferritin and high lipid accumulation) more sensitive vs the poorly differentiated ones. Thus, inhibiting H-ferritin expression or interfering with Warburg effect in poorly differentiated cells could increase their sensitivity towards ferroptosis and enhance the present therapy.

Declaration of competing interest

The authors declare that they have no conflicts of interest.

Acknowledgements

We are grateful to Prof. Antonella Roveri from the University of Padova, for the GPX4 activity quantification. This work was supported by the University of Brescia (ex 60%) research funds to M.P.

R.R. was supported by Associazione Italiana per la Ricerca sul Cancro IG 2019 n° 23151.

M.A. was supported by Associazione Italiana per la Ricerca sul Cancro, AIRC Fellowship, for Italy (two-year fellowship "Loredana Gualandi Sabotti" rif.22482). E.G., M.G. and F.M. were supported by Fondazione Veronesi Fellowship.

Appendix A. Supplementary data

Supplementary data to this article can be found online at https://doi.org/10.1016/j.freeradbiomed.2021.04.024.

Author contribution

M.A. Investigation, Data curation and Writing–original draft. S.B., E.G., M.G., F.M. and L.C. Investigation. R.R. Investigation and review & editing. A.S., G.D.P., P.A., S.M. review & editing. M.P. Conceptualization, Supervision, Data curation, Writing–original draft; Writing–review & editing.

References

[1] S.J. Dixon, K.M. Lemberg, M.R. Lamprecht, R. Skouta, E.M. Zaitsev, C.E. Gleason, D.N. Patel, A.J. Bauer, A.M. Cantley, W.S. Yang, B. Morrison, B.R. Stockwell, Ferroptosis: an iron-dependent form of nonapoptotic cell death, Cell 149 (5) (2012) 1060–1072.

[2] S. Doll, B. Proneth, Y.Y. Tyurina, E. Panzilius, S. Kobayashi, I. Ingold, M. Irmler, J. Beckers, M. Aichler, A. Walch, H. Prokisch, D. Trümbach, G. Mao, F. Qu, H. Bayir, J. Füllekrug, C.H. Scheel, W. Wurst, J.A. Schick, V.E. Kagan, J.P. Angeli, M. Conrad, ACSL4 dictates ferroptosis sensitivity by shaping cellular lipid composition, Nat. Chem. Biol. 13 (1) (2017) 91–98.

[3] R.L. Bertrand, Iron accumulation, glutathione depletion, and lipid peroxidation must occur simultaneously during ferroptosis and are mutually amplifying events, Med. Hypotheses 101 (2017) 69–74.

[4] M.M. Gaschler, B.R. Stockwell, Lipid peroxidation in cell death, Biochem. Biophys. Res. Commun. 482 (3) (2017) 419–425.

[5] B.R. Stockwell, X. Jiang, The chemistry and biology of ferroptosis, Cell Chem Biol 27 (4) (2020) 365–375.

[6] B. Do Van, F. Gouel, A. Jonneaux, K. Timmerman, P. Gelé, M. Pétrault, M. Bastide, C. Laloux, C. Moreau, R. Bordet, D. Devos, J.C. Devedjian, Ferroptosis, a newly characterized form of cell death in Parkinson's disease that is regulated by PKC, Neurobiol. Dis. 94 (2016) 169–178.

[7] W.S. Hambright, R.S. Fonseca, L. Chen, R. Na, Q. Ran, Ablation of ferroptosis regulator glutathione peroxidase 4 in forebrain neurons promotes cognitive impairment and neurodegeneration, Redox Biol 12 (2017) 8–17.

[8] W. Tonnus, A. Linkermann, Death is my heir"–ferroptosis connects cancer pharmacogenomics and ischemia-reperfusion injury, Cell Chem Biol 23 (2) (2016) 202–203.

[9] S.W. Alvarez, V.O. Sviderskiy, E.M. Terzi, T. Papagiannakopoulos, A.L. Moreira, S. Adams, D.M. Sabatini, K. Birsoy, R. Possemato, NFS1 undergoes positive selection in lung tumours and protects cells from ferroptosis, Nature 551 (7682) (2017) 639–643.

[10] S. Hao, J. Yu, W. He, Q. Huang, Y. Zhao, B. Liang, S. Zhang, Z. Wen, S. Dong, J. Rao, W. Liao, M. Shi, Cysteine dioxygenase 1 mediates erastin-induced ferroptosis in human gastric cancer cells, Neoplasia 19 (12) (2017) 1022–1032.

[11] Y. Kinowaki, M. Kurata, S. Ishibashi, M. Ikeda, A. Tatsuzawa, M. Yamamoto, O. Miura, M. Kitagawa, K. Yamamoto, Glutathione peroxidase 4 overexpression inhibits ROS-induced cell death in diffuse large B-cell lymphoma, Lab. Invest. 98 (5) (2018) 609–619.

[12] C. Louandre, Z. Ezzoukhry, C. Godin, J.C. Barbare, J.C. Mazière, B. Chauffert, A. Galmiche, Iron-dependent cell death of hepatocellular carcinoma cells exposed to sorafenib, Int. J. Canc. 133 (7) (2013) 1732–1742.

[13] C. Louandre, I. Marcq, H. Bouhlal, E. Lachaier, C. Godin, Z. Saidak, C. François, D. Chatelain, V. Debuysscher, J.C. Barbare, B. Chauffert, A. Galmiche, The retinoblastoma (Rb) protein regulates ferroptosis induced by sorafenib in human hepatocellular carcinoma cells, Canc. Lett. 356 (2 Pt B) (2015) 971–977.

[14] G.O. Latunde-Dada, Ferroptosis: role of lipid peroxidation, iron and ferritinophagy, Biochim. Biophys. Acta Gen. Subj. 1861 (8) (2017) 1893–1900.

[15] S.J. Dixon, B.R. Stockwell, The hallmarks of ferroptosis, Annu. Rev. Cell Biol. 3 (1) (2019) 35–54.

[16] B. Hassannia, P. Vandenabeele, T. Vanden Berghe, Targeting ferroptosis to iron out cancer, Canc. Cell 35 (6) (2019) 830–849.

[17] S.J. Dixon, D.N. Patel, M. Welsch, R. Skouta, E.D. Lee, M. Hayano, A.G. Thomas, C. E. Gleason, N.P. Tatonetti, B.S. Slusher, B.R. Stockwell, Pharmacological inhibition of cystine-glutamate exchange induces endoplasmic reticulum stress and ferroptosis, Elife 3 (2014), e02523.

[18] S. Doll, F.P. Freitas, R. Shah, M. Aldrovandi, M.C. da Silva, I. Ingold, A.G. Grocin, T. N. Xavier da Silva, E. Panzilius, C.H. Scheel, A. Mourão, K. Buday, M. Sato, J. Wanninger, T. Vignane, V. Mohana, M. Rehberg, A. Flatley, A. Schepers, A. Kurz, D. White, M. Sauer, M. Sattler, E.W. Tate, W. Schmitz, A. Schulze, V. O'Donnell, B. Proneth, G.M. Popowicz, D.A. Pratt, J.P.F. Angeli, M. Conrad, FSP1 is a glutathione-independent ferroptosis suppressor, Nature 575 (7784) (2019) 693–698.

[19] K. Bersuker, J.M. Hendricks, Z. Li, L. Magtanong, B. Ford, P.H. Tang, M.A. Roberts, B. Tong, T.J. Maimone, R. Zoncu, M.C. Bassik, D.K. Nomura, S.J. Dixon, J. A. Olzmann, The CoQ oxidoreductase FSP1 acts parallel to GPX4 to inhibit ferroptosis, Nature 575 (7784) (2019) 688–692.

[20] T. Krainz, M.M. Gaschler, C. Lim, J.R. Sacher, B.R. Stockwell, P. Wipf, A mitochondrial-targeted nitroxide is a potent inhibitor of ferroptosis, ACS Cent. Sci. 2 (9) (2016) 653–659.

[21] A. Jelinek, L. Heyder, M. Daude, M. Plessner, S. Krippner, R. Grosse, W. E. Diederich, C. Culmsee, Mitochondrial rescue prevents glutathione peroxidase-dependent ferroptosis, Free Radic. Biol. Med. 117 (2018) 45–57.

[22] M.M. Gaschler, F. Hu, H. Feng, A. Linkermann, W. Min, B.R. Stockwell, Determination of the subcellular localization and mechanism of action of ferrostatins in suppressing ferroptosis, ACS Chem. Biol. 13 (4) (2018) 1013–1020.

[23] M. Gao, J. Yi, J. Zhu, A.M. Minikes, P. Monian, C.B. Thompson, X. Jiang, Role of mitochondria in ferroptosis, Mol. Cell. 73 (2) (2019) 354–363, e3.

[24] E. Park, S.W. Chung, ROS-mediated autophagy increases intracellular iron levels and ferroptosis by ferritin and transferrin receptor regulation, Cell Death Dis. 10 (11) (2019) 822.

[25] S. Mumbauer, J. Pascual, I. Kolotuev, F. Hamaratoglu, Ferritin heavy chain protects the developing wing from reactive oxygen species and ferroptosis, PLoS Genet. 15 (9) (2019), e1008396.

[26] J. Du, Y. Zhou, Y. Li, J. Xia, Y. Chen, S. Chen, X. Wang, W. Sun, T. Wang, X. Ren, Y. An, K. Lu, W. Hu, S. Huang, J. Li, X. Tong, Y. Wang, Identification of Frataxin as a regulator of ferroptosis, Redox Biol 32 (2020) 101483.

[27] X. Fang, Z. Cai, H. Wang, D. Han, Q. Cheng, P. Zhang, F. Gao, Y. Yu, Z. Song, Q. Wu, P. An, S. Huang, J. Pan, H.Z. Chen, J. Chen, A. Linkermann, J. Min, F. Wang, Loss of Cardiac Ferritin H Facilitates Cardiomyopathy via Slc7a11-Mediated Ferroptosis, Circ Res, 2020.

[28] J.D. Mancias, L. Pontano Vaites, S. Nissim, D.E. Biancur, A.J. Kim, X. Wang, Y. Liu, W. Goessling, A.C. Kimmelman, J.W. Harper, Ferritinophagy via NCOA4 is

required for erythropoiesis and is regulated by iron dependent HERC2-mediated proteolysis, Elife 4 (2015).
[29] M. Gryzik, M. Asperti, A. Denardo, P. Arosio, M. Poli, NCOA4-mediated ferritinophagy promotes ferroptosis induced by erastin, but not by RSL3 in HeLa cells, Biochim. Biophys. Acta Mol. Cell Res. 1868 (2) (2021) 118913.
[30] H. Feng, K. Schorpp, J. Jin, C.E. Yozwiak, B.G. Hoffstrom, A.M. Decker, P. Rajbhandari, M.E. Stokes, H.G. Bender, J.M. Csuka, P.S. Upadhyayula, P. Canoll, K. Uchida, R.K. Soni, K. Hadian, B.R. Stockwell, Transferrin receptor is a specific ferroptosis marker, Cell Rep. 30 (10) (2020) 3411–3423, e7.
[31] C. Mukherjee, T. Kling, B. Russo, K. Miebach, E. Kess, M. Schifferer, L.D. Pedro, U. Weikert, M.K. Fard, N. Kannaiyan, M. Rossner, M.L. Aicher, S. Goebbels, K. A. Nave, E.M. Krämer-Albers, A. Schneider, M. Simons, Oligodendrocytes Provide Antioxidant Defense Function for Neurons by Secreting Ferritin Heavy Chain, Cell Metab, 2020.
[32] W. Hou, Y. Xie, X. Song, X. Sun, M.T. Lotze, H.J. Zeh 3rd, R. Kang, D. Tang, Autophagy promotes ferroptosis by degradation of ferritin, Autophagy 12 (8) (2016) 1425–1428.
[33] P. Arosio, L. Elia, M. Poli, Ferritin, Cellular Iron Storage and Regulation, IUBMB Life, 2017.
[34] I. Grossi, B. Arici, N. Portolani, G. De Petro, A. Salvi, Clinical and biological significance of miR-23b and miR-193a in human hepatocellular carcinoma, Oncotarget 8 (4) (2017) 6955–6969.
[35] A. Roveri, M. Maiorino, C. Nisii, F. Ursini, Purification and characterization of phospholipid hydroperoxide glutathione peroxidase from rat testis mitochondrial membranes, Biochim. Biophys. Acta 1208 (2) (1994) 211–221.
[36] F.A. Ran, P.D. Hsu, J. Wright, V. Agarwala, D.A. Scott, F. Zhang, Genome engineering using the CRISPR-Cas9 system, Nat. Protoc. 8 (11) (2013) 2281–2308.
[37] F. Sivandzade, A. Bhalerao, L. Cucullo, Analysis of the mitochondrial membrane potential using the cationic JC-1 dye as a sensitive fluorescent probe, Bio Protoc 9 (1) (2019).
[38] D. Basuli, L. Tesfay, Z. Deng, B. Paul, Y. Yamamoto, G. Ning, W. Xian, F. McKeon, M. Lynch, C.P. Crum, P. Hegde, M. Brewer, X. Wang, L.D. Miller, N. Dyment, F. M. Torti, S.V. Torti, Iron addiction: a novel therapeutic target in ovarian cancer, Oncogene 36 (29) (2017) 4089–4099.
[39] J. Tsoi, L. Robert, K. Paraiso, C. Galvan, K.M. Sheu, J. Lay, D.J.L. Wong, M. Atefi, R. Shirazi, X. Wang, D. Braas, C.S. Grasso, N. Palaskas, A. Ribas, T.G. Graeber, Multi-stage differentiation defines melanoma subtypes with differential vulnerability to drug-induced iron-dependent oxidative stress, Canc. Cell 33 (5) (2018) 890–904, e5.
[40] A. Forner, M. Reig, J. Bruix, Hepatocellular carcinoma, Lancet 391 (10127) (2018) 1301–1314.
[41] A. Villanueva, Hepatocellular carcinoma, N. Engl. J. Med. 380 (15) (2019) 1450–1462.
[42] T. Amann, U. Maegdefrau, A. Hartmann, A. Agaimy, J. Marienhagen, T.S. Weiss, O. Stoeltzing, C. Warnecke, J. Schölmerich, P.J. Oefner, M. Kreutz, A.K. Bosserhoff, C. Hellerbrand, GLUT1 expression is increased in hepatocellular carcinoma and promotes tumorigenesis, Am. J. Pathol. 174 (4) (2009) 1544–1552.
[43] C.C. Wong, S.L. Au, A.P. Tse, I.M. Xu, R.K. Lai, D.K. Chiu, L.L. Wei, D.N. Fan, F. H. Tsang, R.C. Lo, C.M. Wong, I.O. Ng, Switching of pyruvate kinase isoform L to M2 promotes metabolic reprogramming in hepatocarcinogenesis, PloS One 9 (12) (2014), e115036.
[44] D.F. Calvisi, C. Wang, C. Ho, S. Ladu, S.A. Lee, S. Mattu, G. Destefanis, S. Delogu, A. Zimmermann, J. Ericsson, S. Brozzetti, T. Staniscia, X. Chen, F. Dombrowski, M. Evert, Increased lipogenesis, induced by AKT-mTORC1-RPS6 signaling, promotes development of human hepatocellular carcinoma, Gastroenterology 140 (3) (2011) 1071–1083.
[45] H. Suzuki, M. Kohjima, M. Tanaka, T. Goya, S. Itoh, T. Yoshizumi, M. Mori, M. Tsuda, M. Takahashi, M. Kurokawa, K. Imoto, S. Tashiro, A. Kuwano, M. Kato, S. Okada, M. Nakamuta, Y. Ogawa, Metabolic alteration in hepatocellular carcinoma: mechanism of lipid accumulation in well-differentiated hepatocellular carcinoma, Chin. J. Gastroenterol. Hepatol. 2021 (2021) 8813410.
[46] P. Arosio, R. Ingrassia, P. Cavadini, Ferritins: a family of molecules for iron storage, antioxidation and more, Biochim. Biophys. Acta 1790 (7) (2009) 589–599.
[47] M. Fujimaki, N. Furuya, S. Saiki, T. Amo, Y. Imamichi, N. Hattori, Iron supply via NCOA4-mediated ferritin degradation maintains mitochondrial functions, Mol. Cell Biol. 39 (14) (2019).